recycling

MDPI

Article

Towards Closed-Loop Aerospace Waste Recycling: FAST Nickel Superalloy Tooling for Direct Titanium Waste-to-Wire Continuous Extrusion

Lucas Cook *, Samuel Lister, William Pulfrey, Eric Goodall and Martin Jackson

School of Chemical, Materials and Biological Engineering, The University of Sheffield, Mappin Street, Sheffield S1 3JD, UK; sam.lister@sheffield.ac.uk (S.L.); will.pulfrey@sheffield.ac.uk (W.P.); eric.goodall@sheffield.ac.uk (E.G.); martin.jackson@sheffield.ac.uk (M.J.)
* Correspondence: ltcook1@sheffield.ac.uk

Abstract

With increasing interest in wire additive technologies for titanium parts, there is increasing demand for low-cost wire from secondary sources, of which there is an abundance. In this investigation, both machining swarf and out-of-specification AM commercially pure titanium alloy powder have been successfully consolidated into wire using the solid-state CONFORM™ continuous extrusion process. Such wire from secondary sources has been directly compared with solid bar feedstock. Historically, one of the key challenges was the wear of CONFORM™ tooling. In this study, nickel superalloy waste powder was fully consolidated through the field-assisted sintering technology (FAST) to create novel recycled tooling. This study demonstrates the effect of the continuous extrusion process directly on each feed material and how the use of multiple sources of secondary aerospace waste can allow such a process to operate within a closed-loop recycling system. Machining swarf has been demonstrated to be a viable feedstock for wire production via the CONFORM™ process coupled with the use of recycled nickel superalloy tooling. Such metal circularity technology is timely as titanium- and nickel-based superalloy aerospace waste is predicted to increase over the next two decades to meet future aircraft build demands.

Keywords: titanium; continuous extrusion; CONFORM™; metal recycling; nickel superalloy; FAST

1. Introduction

Low-cost titanium alloy production has been a key goal for over two decades. Research has focused heavily on trying to replace the Kroll process with significantly cheaper methods of extraction, with little success at the pilot scale [1,2]. However, the greatest change associated with the cost of titanium is from secondary and downstream production [3,4]. Waste materials such as oversized or unusable powders from additive manufacturing or machining swarf (also known as chips or turnings) offer a significant opportunity in the overall cost reduction of titanium alloy parts. This requirement is further compounded economically and environmentally, with the production of critical materials such as titanium from primary sources being heavily affected by inefficient extraction and an unstable global supply chain. Such supply issues have become more problematic due to the Ukraine–Russia conflict. Machining swarf is a particularly interesting feedstock as up to 90% of titanium alloy forgings are machined away for critical aero-engine and aerostructural components [5,6]. This leaves the remaining waste to be devalued and downgraded as it is converted to

Check for updates

Academic Editor: Michele John

Received: 11 September 2026
Revised: 18 October 2026
Accepted: 20 October 2026
Published: 23 October 2026

Copyright: © 2026 by the authors. Licensee MDPI, Basel, Switzerland. This article is an open access article distributed under the terms and conditions of the Creative Commons Attribution (CC BY) license.

ferrotitanium as an automotive steel manufacturing alloy addition. In this study, the aim is to convert this secondary titanium swarf back into wire in order to retain its aerospace value and excellent properties.

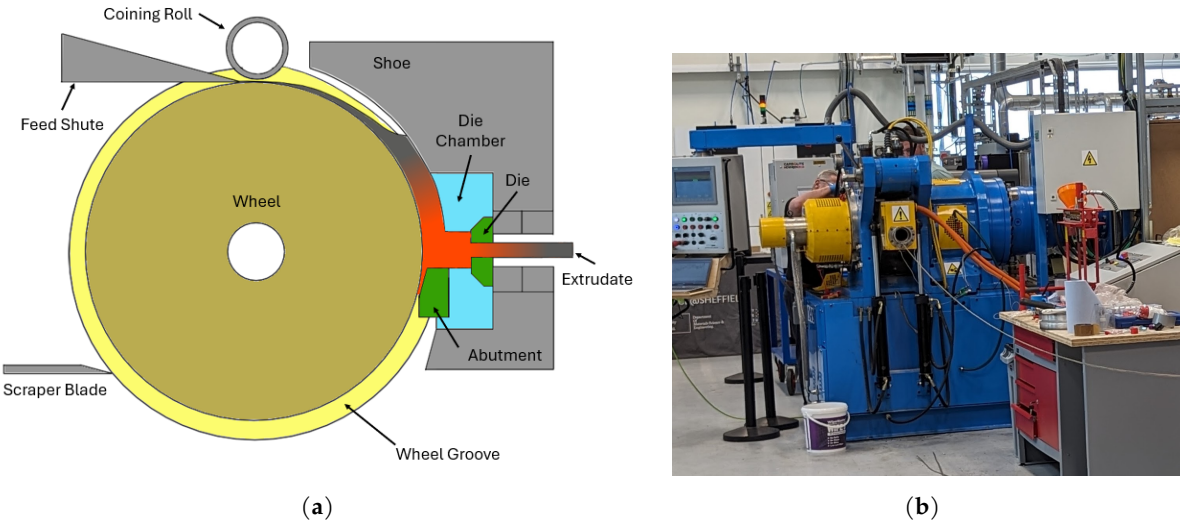
There are two main avenues of research that aim to reduce the waste and costs associated with titanium production, and both relate to near-net-shape manufacturing. One route is hybrid processing, and the other is the increased use of additive manufacturing processes with increased design freedoms and overall superior economics over other processes [7]. One of the major possibilities with AM techniques in the direct energy deposition field is the use of waste materials to produce feedstocks for techniques such as wire arc additive manufacturing (WAAM) or additive friction stir deposition (AFSD). WAAM claims to offer economic advantages over laser powder bed fusion (LBPF) processes [8]. If these advantages can be further exploited, it can lead to further use of the process and more cost reductions for produced parts [8,9]. There is great interest in processes that can take this waste material and produce wire feedstock for future aerostructural parts.

Friction extrusion (FE) is a batch process that relies on severe plastic deformation (SPD) rather than the traditional remelting to consolidate waste material. This process combines the effects of adiabatic heating and stored lattice energy to produce continuous dynamic recrystallization [10–14]. Research into converting Ti-6Al-4V chips into billet produced via FE provided a higher ultimate tensile strength and yield strength than a reference bar [14]. One of the main issues with this process was the additional briquetting step required to consolidate the chips before extrusion. The main industrial limitations of FE relate to the diameter of the produced wire being small and the batch nature of the billets, thereby limiting the material throughput [14]. Another SPD process is equal channel angular processing (ECAP), which relies on an internal channel bent through a 90° angle where rod or swarf material is then forced through the channel and die with a hydraulic ram multiple times to induce SPD through redundant work on the material as it flows through the chamber [13,15,16]. This can achieve grain refinement up to the sub-micron range and produce materials that have exceptionally high strength in comparison to as-produced material [15,17,18]. However, this process comes with multiple limitations; for example, ECAP uses discrete billets that need to be forced through by a hydraulic ram at extremely high loads. This limits the scalability of production as the requirement for the hydraulic ram does not allow continuous processing of material. While the billets can be increased in size to increase production, the lack of a continuous feed limits the future industrial application of ECAP as secondary to continuous production processes. One such process that allows future industrial scalability and consolidation directly from swarf is continuous extrusion, such as CONFORM™ [14,19,20].

The main advantage of continuous extrusion over conventional SPD processes is that it removes the need to can in steel as material can be fed directly into the machine at room temperature and produce any wire indefinitely as long as the tooling retains good structural integrity [21]. A range of feedstocks can be used from conventional bar stock through to powder and granules [22,23]. This feedstock is fed directly into a groove within an extrusion wheel until it is pressed into an abutment and enough friction and back pressure are developed ahead of the die chamber. The material is then extruded through a profiled die [24,25]. This process is schematically illustrated in Figure 1a for powder/swarf feeds. Figure 1b shows the powder-derived wire being extruded via CONFORM™ at the University of Sheffield. Powder and swarf need no pre-consolidation before the extrusion process [24,25].

CONFORM™ has historically processed mainly lower-strength materials such as aluminum and copper, both from bar and particulate feeds, with only minor alterations, such as flow-controlled hoppers fitted to the machine to accommodate the particulate feeds [22,26].

There are currently few examples of higher-strength metals such as titanium being produced via continuous extrusion, especially when it comes to production via powder or particulate feeds [23,27]. Most publicly available research is on the production of wire from initial rod feed.



(**a**) (**b**)

Figure 1. (**a**) Schematic of the feed mechanism and extrusion areas of the CONFORM™ machine. (**b**) Photograph of the CONFORM™ machine as it is extruding 5 mm CP-Ti Gr2 wire.

One interesting aim of research into continuous extrusion processes has been the possibility of producing titanium wire via powder or swarf (machining waste) feedstocks. The initial investigations into this process were carried out at the University of Sheffield [23]. This research found that wire produced via CONFORM™ with CP-Ti Gr2 titanium powder produced fully dense wire with a fine-grain microstructure due to the severe plastic deformation during the CONFORM™ continuous extrusion process.

Further research investigated the possibility of producing wire from titanium waste sources such as oversized AM powder and machining swarf [27]. Wire was produced from three sources during this research. CP-Ti Gr2 powder was processed for initial tooling preparation, followed by CP-Ti Gr2 swarf and then Ti-6Al-4V machining swarf. As a result of these trials, various lengths of wire from the different feedstocks were produced, characterized and tested against conventional wire to demonstrate the improved performance of both the CP-Ti and Ti-6Al-4V swarf-produced wire. Furthermore, the wire was then cold drawn to show the possibility of downstream use within wire additive manufacturing and welding processes [27].

In addition to the consolidation of waste titanium feedstocks in the CONFORM™ process itself, the sustainability credentials could be further increased by producing part of the tooling assembly (such as the abutment) from nickel superalloy powder, classified as out of specification for AM processes due to the narrow size fraction and morphology tolerance in powder AM routes. Field-assisted sintering technology (FAST) has been shown to be highly tolerant to feedstock morphology and has been proven as an effective solid-state recycling route for titanium machining swarf [28], with an optional post-forging step (FAST-forge) [28]. The authors demonstrate that FAST could be used in the near future to produce sustainable CONFORM™ tooling from nickel superalloy machining waste in a minimum of three steps (clean–FAST–machine).

The Proposed Two-Step Closed-Loop Recycling Approach

Figure 2 schematically demonstrates the proposed two-step approach for recycling aerospace waste. Step 1: Tap into the increasing stockpile of nickel superalloy powder (unusable for AM) to create novel CONFORM™ abutment tooling via FAST. FAST has

previously been demonstrated as an effective method for consolidating one or more nickel superalloy powders [29–32], producing microstructures and properties that are consistent with conventionally forged material. It has also demonstrated reductions in processing time and the need for encapsulation prior to consolidation [33]. Step 2: Utilise the ever increasing amount of titanium waste as feedstock to use within CONFORM™ to produce wire.

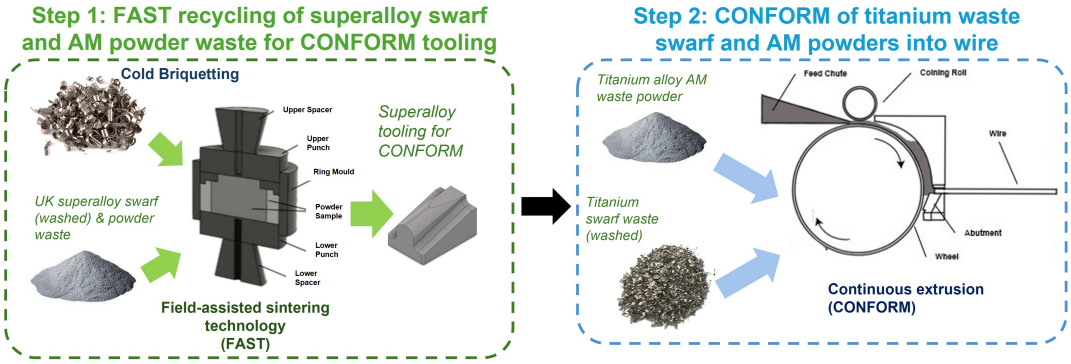


Figure 2. Diagram illustrating the proposed route towards closed-loop recycling approach for nickel superalloy and titanium aerospace waste in order to produce low-cost wire.

2. Materials and Methods

2.1. CONFORM™ Tooling

A BWE 315i CONFORM™ machine located at the Royce Translational Centre, the University of Sheffield, Sheffield, UK, was adapted for particulate feed. This included: (1) changes to conventional CONFORM™ tooling to enable powder and swarf feeds, (2) a new particulate feed system, and (3) nickel superalloy abutment to increase tooling life when processing titanium waste streams. This abutment development was driven by the original tooling materials not being suitable for the production of titanium as the wear rates on the abutments are too high for economical wire production. For the production of the abutments, FAST was used to consolidate out-of-specification AM powder into billets, from which a number of abutments were machined.

2.2. FAST Process of Nickel Superalloy Powder

The powder was processed using an FCT HP D 250C (Frankenblick, Germany) FAST furnace at the Royce Discovery Centre, University of Sheffield. The powder was a proprietary precipitation-strengthened nickel-based superalloy. The procedure for producing the billets is as follows: a graphite ring die, as shown in Figure 3a, is lined with a layer of graphite foil. A cylindrical graphite punch was then partially inserted into the ring. Three 120 mm diameter graphite foil discs were then inserted into the ring above the punch. Then, 5 kg of powder was poured into the ring die, and then three further graphite foil discs were placed above the powder. A second cylindrical graphite punch was then inserted into the top of the ring, which completed the full die assembly. Graphite foil used during the process helps with specimen removal and helps to prevent any parts of the assembly from bonding together, further reducing the wear in the graphite tooling. A graphite felt jacket is also used around the die assembly to reduce the radiative heat loss of the die assembly. The full assembly of the graphite tooling stack is shown in Figure 3b. The die assembly was then placed in the FAST machine between the two hydraulic rams, which are conductive. All this is contained within the furnace's vacuum chamber, and an initial load is then applied to ensure that there is enough contact between ram and die to generate an electrical contact. Conical graphite supports are used to adapt the diameter of the ram to the diameter of the graphite punches. Further, 5 kg of nickel superalloy powder, with

a particle size distribution >53 µm, was consolidated into a billet. The sintering process took place under vacuum whilst a uniaxial pressure of 35 MPa and dwell temperature of 1150 °C for 40 min were applied through a Joule heating effect caused by the resistance to the flow of a pulsed DC current through the graphite tooling stack and nickel superalloy powder. The entire powder consolidation process took less than 2 h. The average heating rate from 300 °C to 1150 °C was 34 °C/min. The average cooling rate from 1150 °C to 600 °C was 9 °C/min, then allowed to freely cool within the vacuum chamber. Evidence of full consolidation is observed in Figure 3c, which then allowed several abutments to be extracted via conventional machining processes. Examples of the abutments that are machined out of the consolidated billets can be seen in Figure 3d.

2.3. Continuous Extrusion of Titanium Feedstocks

For the production of the wire from all three CP-Ti Gr2 feedstocks, the die chamber was heated to between 400 and 550 °C using an in-built induction heater and left for 30 min to allow the die to heat up and remain at a steady temperature. To warm the wheel before samples were taken for analysis, some of the bar feed was processed through the machine in order to raise the wheel temperature to around 100 °C. This process also facilitated coating the wheel groove with a titanium tire that provides back pressure and aids the continuous extrusion. All the samples were produced within a wheel speed range between 2 and 10 RPM to assess the performance of the abutment to produce wire at differing process speeds.

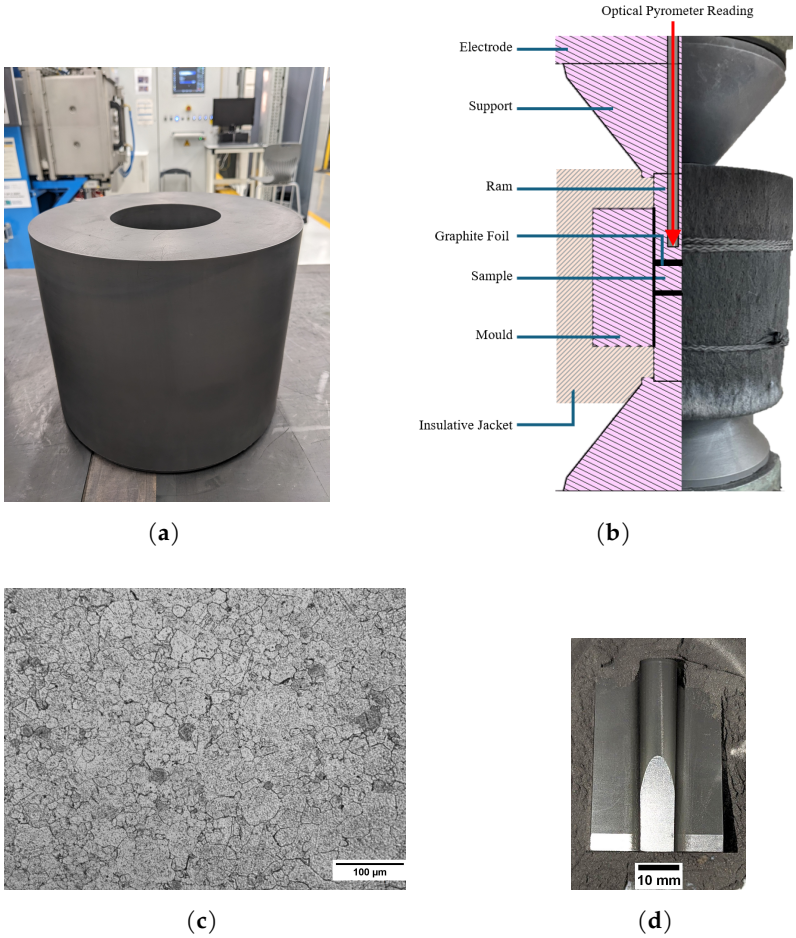


Figure 3. (**a**) Photograph of the graphite tooling used within the FAST process. (**b**) Schematic of the FAST machine tooling arrangement with respect to the sample (taken from [34]). (**c**) Optical micrograph of the nickel superalloy microstructure consolidated via FAST. (**d**) Photograph of a nickel superalloy abutment surrounded by the initial feedstock powder.

2.4. Tensile Testing

Tensile testing was carried out by Element, Sheffield, UK. Testing was carried out on 25 cm lengths for 10 mm diameter wire and 30 cm lengths for the 5 mm diameter wire. Testing was performed in accordance with BS EN 2002-1-2005 [35].

2.5. Chemical Analysis

Chemical analysis was carried out by the Sheffield Assay Office, Sheffield, UK. Three samples from each of the CP-Ti Gr2 wires deriving from the different feedstocks were tested, weighing between 2 and 5 g.

2.6. Metallographic Preparation

Standard titanium alloy preparation routes were followed for all the specimens. Sections of the wire were abrasively sectioned in the areas of interest in the perpendicular and extrusion directions prior to hot mounting in Bakelite. The sections were then ground using progressively finer SiC papers and chemically polished using 0.05 µm colloidal silica with a 10% volume of 30% concentration hydrogen peroxide added.

2.7. Characterization

Micrographs were taken using a Nikon Eclipse LV150 light microscope, Tokyo, Japan, under cross-polarized light mode. For high-resolution analysis, an FEI Inspect F50 microscope, Hilsboro, OR, USA, was used to acquire secondary electron images at an accelerating voltage of 2 kV and a spot size of 3.5. EBSD analysis was performed on a JEOL 7900F field emission gun (FEG) SEM, Tokyo, Japan and an Oxford Instruments Aztec HKL Advanced Symmetry System, High Wycombe, United Kingdom, then processed on Aztec Crystal. Data was acquired at 20 kV and a step size ranging from 10 to 100 nm depending on the feedstock.

2.8. Post-Extrusion Heat Treatments

Sample heat treatments were performed within a Lenton tube furnace, Hope Valley, United Kingdom, under an argon atmosphere. Two treatments were performed on all three extruded wire sets, at 600 °C and 800 °C, for a 3 h dwell prior to an air cool.

2.9. Titanium Feedstocks

Three CP-Ti feedstock types were used in the production of the 5 mm diameter wire: CP-Ti Gr2 titanium bar of a 10 mm diameter from Ti-Tek UK Ltd, Birmingham, United Kingdom and CP-Ti Gr2 HDH powder originally from Reading Alloys, Robesonia, PA, United States. The average size of the powder was around 45 µm and had a very angular morphology; this makes the powder out of specification for AM processes. In addition, the powder that was used in this study was deemed to be unsuitable for a previous study and therefore regarded as waste. This powder has a much more angular morphology than similar powders used for additive manufacturing, which increases the particle interlocking and provides effective back pressure for a given wheel speed, which enhances continuous production. Finally, CP-Ti Gr2 titanium swarf was washed and sieved to <2 mm by Transition Metals, Sheffield, United Kingdom. The initial microstructures and textures for all three feedstocks can be found in Figure 4. Nickel superalloy waste powder was provided by a UK aerospace supply chain company, Glasgow, United Kingdom. The morphology of the swarf helps with continuous extrusion due to the angular and irregular morphology of the particulate. Such swarf particulates interlock together in the wheel groove far more effectively than HDH angular powder, leading to even greater amounts of back pressure ahead of the die chamber. The bar feed material was annealed at 700°C before processing. All the other materials were used in the as-received condition.

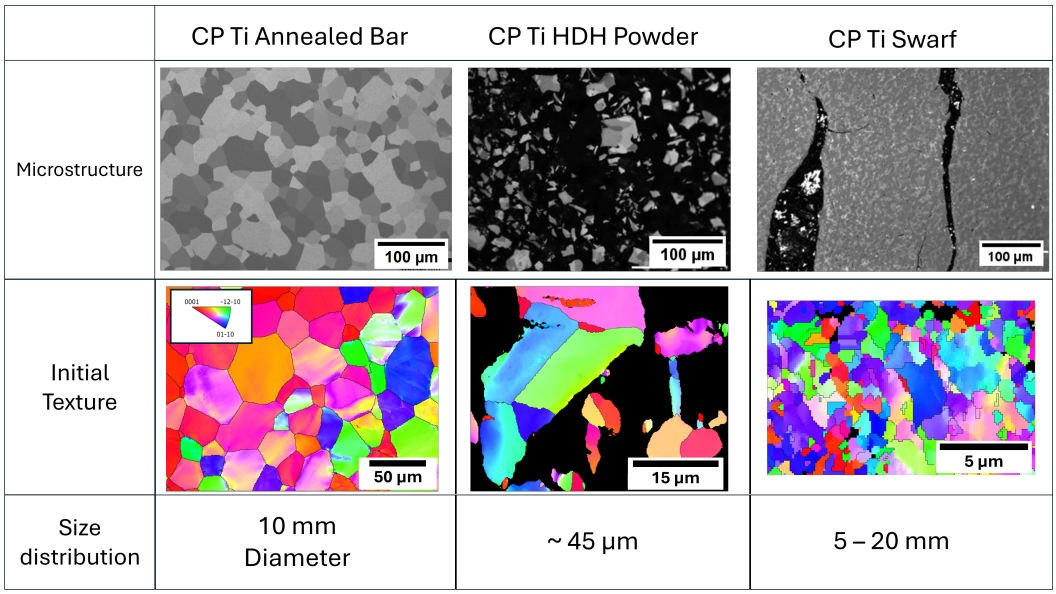


Figure 4. Cross−polarized light micrographs and IPF Z EBSD maps showing the initial microstructure and texture of the CP−Ti Gr2 feedstocks used.

3. Results and Discussion

Previous investigations into the CONFORM™ process have not directly compared the microstructure or mechanical properties of wire produced from bar, powder and swarf. In this study, we are able to assess the effects of continuous extrusion on a range of different titanium waste feedstocks from the initial feedstock morphology to the produced wire. This study measures, for the first time, the effect of the CONFORM™ process on the microstructure and texture evolution of wire deriving from different feedstocks.

Two die sizes were used during this wire production study, a 5 mm die for the bar and powder feeds and a 10 mm die for the swarf feeds. The larger die permitted better consolidation of the irregular feed materials and allowed easier production of the wire from this source. For the powder feed, adjustments were made to the upper die chamber, with a larger protrusion into the wheel groove to allow better pre-compression of the powder, which reduces the amount of unconsolidated powder flowing into the die chamber. The differing die sizes also affect the production of the wire. The 10 mm die was not suited for the fine powder that was used as the powder did not produce enough back pressure in the die chamber and would flow out of the die unconsolidated. The effects on the produced wire are the differing strain rates over the bulk of the material. Due to the smaller diameter the higher strain rates tend to develop further into the wire, causing a comparably finer average grain size within the core of the material. There is little change to the edges of the wire as the strains in this region tend to be consistent.

For the production of all the wire types, it is worth noting that there was no preheating of the feedstock on entry into the CONFORM™ wheel, nor was there any use of inert gas shielding for any exiting wire.

3.1. Finite Element Modeling

A 3D finite element model (FEM) of the CONFORM™ process was created to analyze the material flow and effects of changing tooling on the output of the continuous extrusion process. Material data of Grade 2 titanium was taken from the DEFORM ® software V13.0.1. Various compromises had to be made in order to correctly model the process and reduce computational complexity. For example, feedstock material was modeled as a continuous bar feed and, due to the limitations within the software, could not be modeled with powder

and swarf feeds, so it cannot be directly compared to those produced samples. However, approximations of strain gradients and overall flow can be provided from the DEFORM® models. Various sections of the die and the assembly were modeled as one solid piece to reduce the chance of the nodes within the DEFORM® mesh leaking into the gaps within the model. It is also assumed that, during the process, any material dead zones have already been filled. This is in relation to areas such as the tire coating on the wheel groove and the surface of the abutment, which in CONFORM™ processing usually requires coating when using new tooling. The final assumptions are the continuous temperature of the tooling and the rigidity of the tooling, with no change to the shape and strength of the abutment through the process.

3.2. Continuous Extrusion Using Nickel Superalloy Abutments

During these trials nickel superalloy abutments manufactured via the FAST process were tested under the harshest conditions during the production of titanium wire, particularly at the startup processing stage. During startup, the stress on the abutment is at its highest point due to the relatively low temperatures of the material and any residual material left on the tire of the CONFORM™ wheel. The abutment material withstood a number of startup cycles with limited processing. Following this, the nickel superalloy abutment was tested under the steady-state process where the majority of wire production takes place. This process could range between 30 and 90 m of continuous processing, producing tens of meters of wire before an issue with the feeding system leads to the cessation of the trial. Examples of the wear rates during the trials can be seen in Figure 5. The wear on the abutments is around 1–2 mm after 90 min of consistent processing. Higher wear rates can go as high as 5 mm if consistent processing past startup is not achieved. Titanium build-up on the abutment can also lead to issues with fouling with the wheel and cause damage to the wheel and requires machining away between runs.

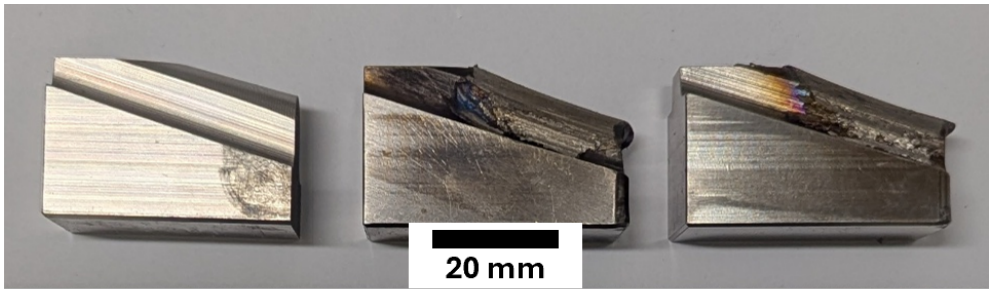


Figure 5. Examples of nickel superalloy abutments. The first is in the as-produced state and two abutments used during titanium extrusion.

3.3. Titanium Wire

A continuous length of several tens of meters of 5 or 10 mm diameter wire was extruded from the CONFORM™ machine. Examples of the lengths produced from these trials can be seen in the photograph in Figure 6a. For each of the three feedstocks the first sections of wire were not taken for analysis as these areas were not produced during the steady-state condition and can have varied microstructures and surface qualities. The surface qualities of the produced wire can be seen in Figure 6b post-extrusion and Figure 6c during extrusion. For both the bar and powder feeds, when viewed under cross-polarized light, the microstructure generally shows an equiaxed microstructure, as can be seen in Figure 7.

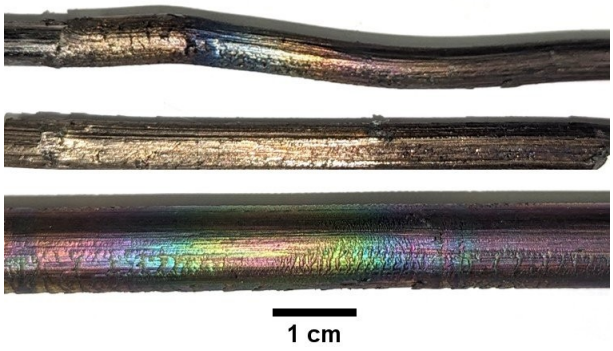
The main difference identified between these two feeds is the homogeneity of the microstructures. At areas along the edge of the sample of the bar, there is very clear grain refinement below the alpha case layer, which then slowly transitions into the homogenous

grain size that can be seen in the core of the wire, as shown in both Figures 7 and 8. This area shows the large effect of the grain refinement of the continuous extrusion process due to the extremely high strain that is generated in these areas. The average grain size in this area is reduced to around an average of ~12–18 ± 6 μm, with the very edge of the sample being reduced to around ~3–5 μm. In the core of the sample there is some grain refinement, with a reduction from ~50 μm to ~30 μm as the strain in the core of the sample is lower than at the edges, as shown in Figure 9. In comparison, the powder sample has a more homogenous microstructure and a refined grain size of 1.23 μm ± 0.7 μm at the edge of the sample and an average grain size of 1.75 μm ± 0.49 at the core of the sample.

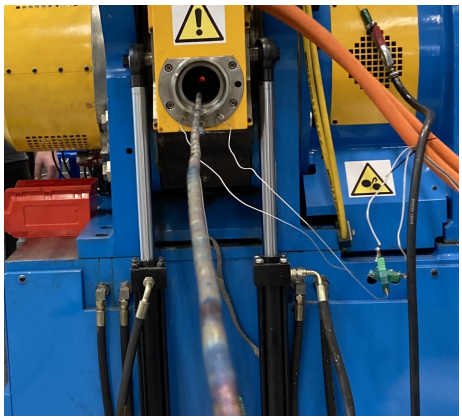
The wire produced from swarf has the most varied microstructure. This is mainly due to the large presence of prior particle boundaries, as shown in Figure 8, predominantly along the edge of the wire. This is likely caused by the more inconsistent pressures that are found along the edges of the die. This creates the most varied grain sizes from the edge to around 1 mm within the microstructure, especially when viewed along the longitudinal direction of the samples. The average grain size at the sample edge is 6.2 μm ± 4 μm. The overall porosity of the powder and swarf wire is relatively low barring the 'onion skin' effect, which can be seen on the powder sample in the longitudinal direction. Once past this 'onion skin' layer into the core of the sample, the microstructure is much more equiaxed and consistent with a much larger grain size than the powder sample. The average grain size in the core of the sample increases to 10.45 μm ± 4.2 μm. Such an effect has been observed in aluminum wire from continuous extrusion [36].



(**a**)



(**b**)



(**c**)

Figure 6. (**a**) Photograph of the authors holding an example of extruded titanium wire derived from machining swarf. (**b**) Image of the surface finish of the wire from all 3 sources. From top to bottom: bar-derived, powder-derived and swarf-derived. (**c**) Photograph of 10 mm wire derived from machining swarf exiting the CONFORM™ machine.

The 'onion skin' is usually caused by a variable particulate feed rate, where not enough particulate material is fed into the groove and the consolidated material remains stagnated

in the die, causing a large amount of heat to be inputted into the sample. Upon extrusion the oxidized surface can cause tearing of the wire. The surface quality of all the wire types is relatively low, as observed in Figure 6b. However, this will not have much of an effect as, with downstream processing such as wire drawing, this brittle oxide layer typically breaks up and spalls away as it enters the wire drawing die, leaving a bright, smooth and consistent finish on the surface of the cold drawn wire [27]. It is currently unknown if the internal microstructural issues such as incomplete consolidation present within the swarf sample will cause any issues with downstream drawing. Further investigations into microstructure after drawing will be performed with future trials.

In addition, downstream cold drawing will break off the oxide surface, leaving a bright finish. Both the swarf and powder samples show the shear flow lines, which are consistent with other materials processed by CONFORM™ due to the differing speeds present within the center and edges of the die causing a large shear force. The powder showed the greatest effect of this with a large number of thin bands along the length of the sample.

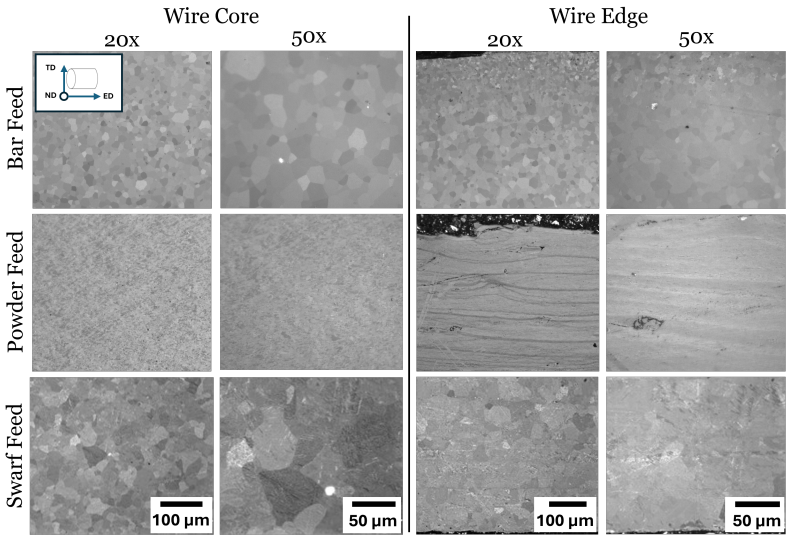


Figure 7. Cross-polarized light micrographs of the extruded wire in the transverse direction, comparing the core of the wire against the wire edge.

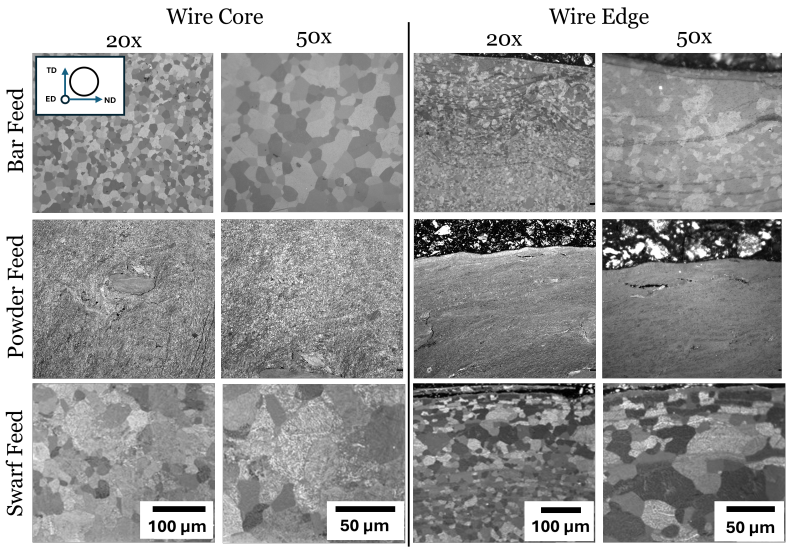
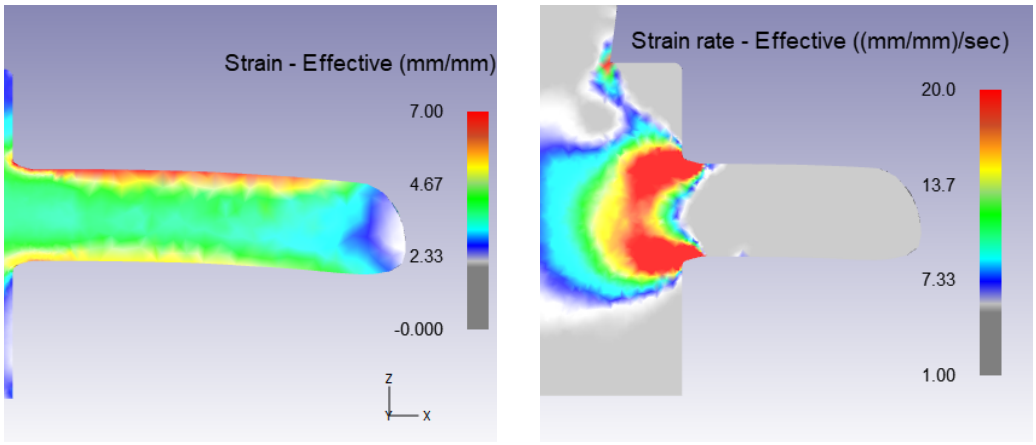


Figure 8. Cross-polarized light micrographs of the extruded CP-Ti Gr2 wire in the extrusion direction, comparing the wire core and edge regions.



(**a**) (**b**)

Figure 9. DEFORM® model of the CONFORM™ process showing, for CP-Ti Gr2 5 mm diameter wire, (**a**) effective strain and (**b**) effective strain rate from a 2D slice of the 3D model.

The results of the microstructures observed under light microscopy are supported by the results shown via the DEFORM® model (Figure 9), with larger-strain regions being seen on the edges of the wire, as supported by the fine microstructures that are seen below the alpha-case layers on the produced bar sample. A secondary confirmation of the DEFORM® model is the flow of the material both into the die and the extruded wire. The flow of material is consistent with what is seen during production in the die chamber. Post-extrusion heat treatments of the wire produced promising results within the bar- and powder-derived samples, as shown in Figure 10. Figure 10a shows the expected full recrystallization. Recrystallization occurred over the majority of the powder-derived wire. There were very few areas of remaining prior powder particles, predominantly towards the edge of the wire, as shown in Figure 10b. There was an area of finer microstructure still present around the edge of the sample inside of the alpha case layer, as shown in Figure 10b. This was somewhat expected to remain after heat treatment due to the high strains and dislocations in this area, which would inhibit grain growth and favor recrystallization. This will be removed before downstream processing due to the higher oxygen content, which is undesirable.

Upon inspection of the wire derived from swarf after heat treatments, shown in Figure 10c, some interesting observations were found. In the core of the sample there is a mostly uniform grain growth with a uniform equiaxed microstructure. The grain size was not entirely uniform as there was evidence of some larger grains within the microstructure. However, this was likely due to the initial microstructure in this area rather than specifically an effect of the heat treatments. The most significant observation was found at the edge of both the extrusion and transverse directions. In the extrusion direction below the large grained alpha case layer was a secondary layered structure of both fine grains and large grains that showed very little evidence of recrystallization.

The EBSD analysis of the three samples highlights the effect of the continuous extrusion process on the texture of the produced samples. This is seen in Figures 11a and 12, where the bar-based wire edge has very strong texture in the normal direction with very little effect on the texture from the extrusion. There are some small areas towards the edge where texture aligned to the extrusion direction is more prominent, but these areas are quite small. In the powder-derived wire, this effect on textural evolution is almost completely reversed, with a noticeable difference between the top and bottom wire edges; the top edge of the sample is almost entirely preferentially aligned towards the extrusion direction, whereas the bottom edge is largely oriented in a mixture of extrusion and transverse directions, as

can be seen in Figures 11a and 13. The core of the powder sample, favorably towards the bottom edge, tends to have strong directionality towards the extrusion direction. It is likely that it follows this pattern as the centre of the wire usually flows out much more quickly during extrusion. Interestingly the size of the textured regions follows closely to the strain profiles that are produced from the DEFORM® model (Figure 9). However, as this is not the case for the bar sample, it cannot be determined whether this is a byproduct of this process specifically for powder samples or if there is not enough strain to introduce this preferential directionality completely within the bar samples or this is simply just a trend that is seen within just this sample. Evidence of the flow lines for the powder sample shown in Figure 11b can also be seen in Figure 11a, with a small band of directionality towards the normal direction flowing through an area preferential towards the extrusion direction.

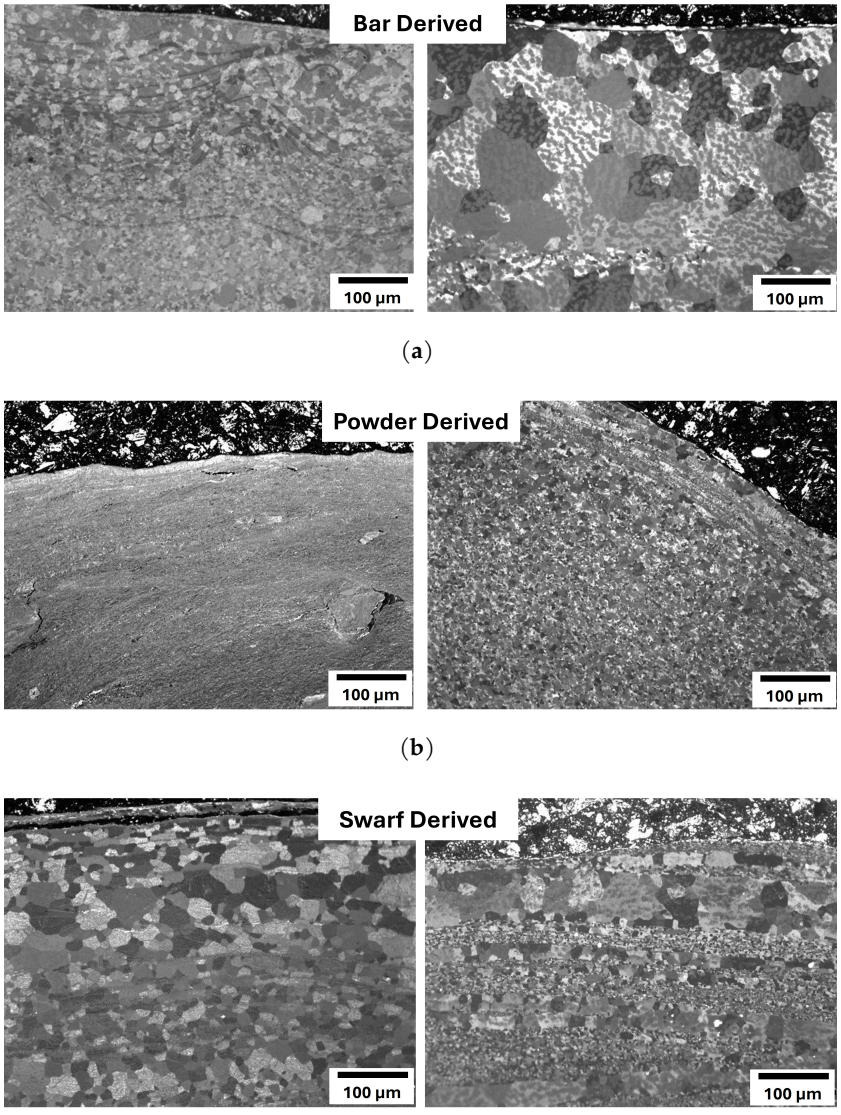


Figure 10. Light micrographs of all 3 wire samples before heat treatment (left) and after heat treatment (right). (**a**) Bar derived wire, (**b**) Powder derived wire, (**c**) Swarf derived wire

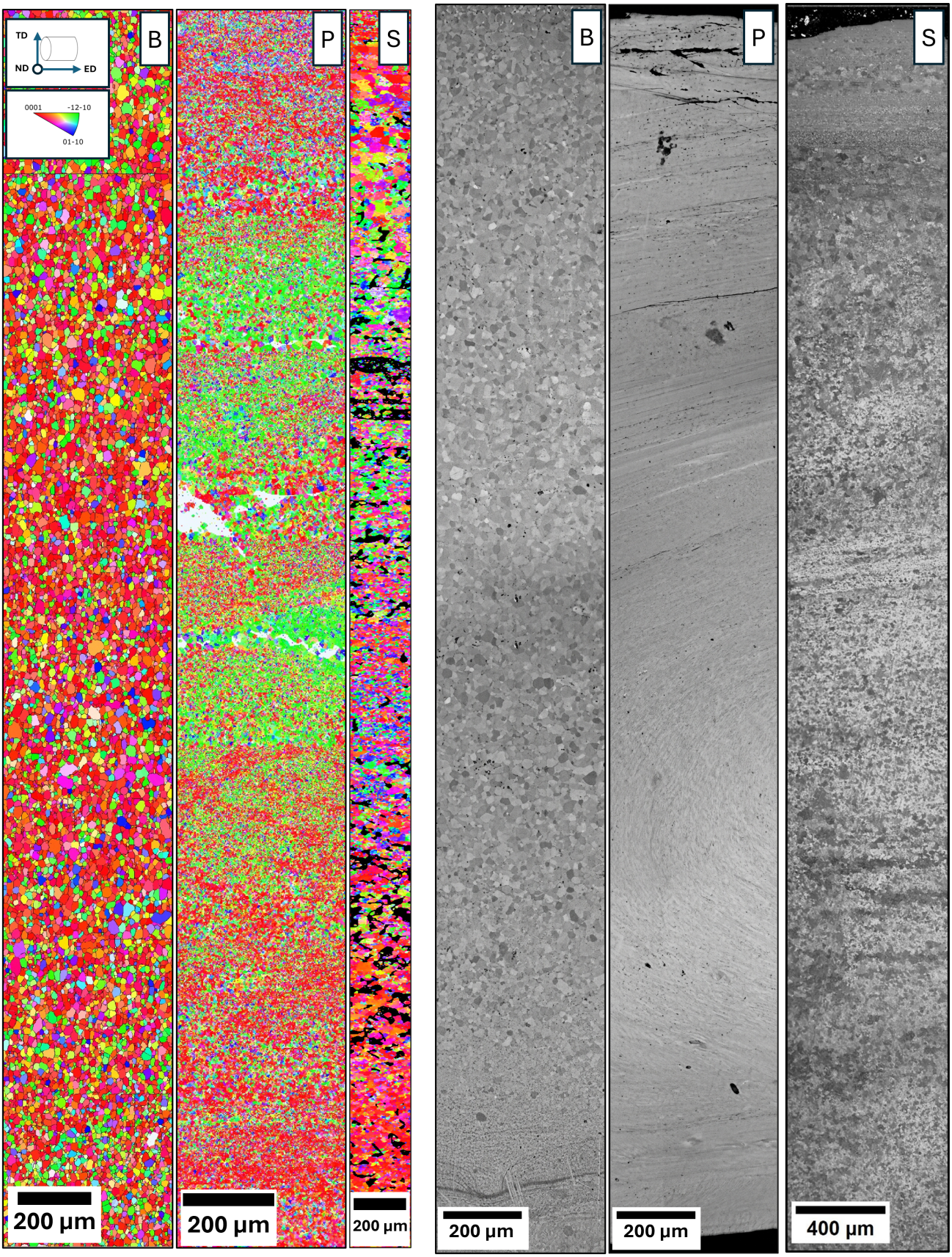
The powder samples also show evidence of prior powder particles remaining within the bulk material that have not recrystallized into the surrounding areas, as can be seen in Figure 12a,b, but it is more predominant in the transverse direction. This is not to say that these particles have not diffusion bonded together; there is no evidence of porosity or lack of bonding between these areas. For the swarf sample the 'onion skin' effect is clearly

visible in Figure 10c and highlights the difference in grain size between the layers where prior swarf particles have not undergone the dynamic recrystallization in a very similar way to the powder particles. The difference in grain sizes between these areas can range from up to 30 μm in the coarse-grain regions down to 1 μm in the fine-grain regions, as can be seen most clearly in Figure 12a. The texture is also heavily influenced by the recrystallization; the areas where the prior swarf particles have not recrystallized retain the texture of the prior swarf particle. This is especially evident in the transverse samples where there is little to no order of the texture and shows the varied textures of the prior swarf particles that can be seen within the wire in both the transverse and parallel directions in Figure 12a,b. The powder-derived wire showed two distinct orientations between the edges and the core of the wire. The edges of the wire show a texture oriented towards the extrusion direction in these higher-strain regions, as can be seen in Figure 13. At the core of the wire, there is a much stronger texture normal to the extrusion direction, with a minor region of the banding showing an extrusion orientation. This is likely a result of the varied strain rate between the edges and the core of the wire, leading to distinct regions within the sample. Interestingly, the texture on the edges of the swarf-derived wire shares similarities to that at the edges of the powder-derived wire. However, at the core of the sample, there is much less directionality and a random texture outside of some of the banding regions. It is likely that the lower strain in these regions has not overcome the original texture of the swarf particles and they have retained their original texture. This demonstrates that the wire produced from swarf, at least at these lower wheel speeds, will have a more isotropic nature at the core of the wire than that of the powder.

A chemical analysis of the three extruded wires, as shown in Table 1, provides very positive results regarding the wire produced via swarf, with the three analysed samples having an average oxygen content of around 0.11 wt.%. When comparing this with the bar samples with an average of around 0.17 wt.% this is further evidence that production from swarf is a viable route for recycling with minimal oxygen pickup. However, the powder-derived wire had a much higher oxygen content at an average of 0.41 wt.%. This helps to explain the brittle nature of this wire alongside the very fine-grain microstructure seen in these wire samples.

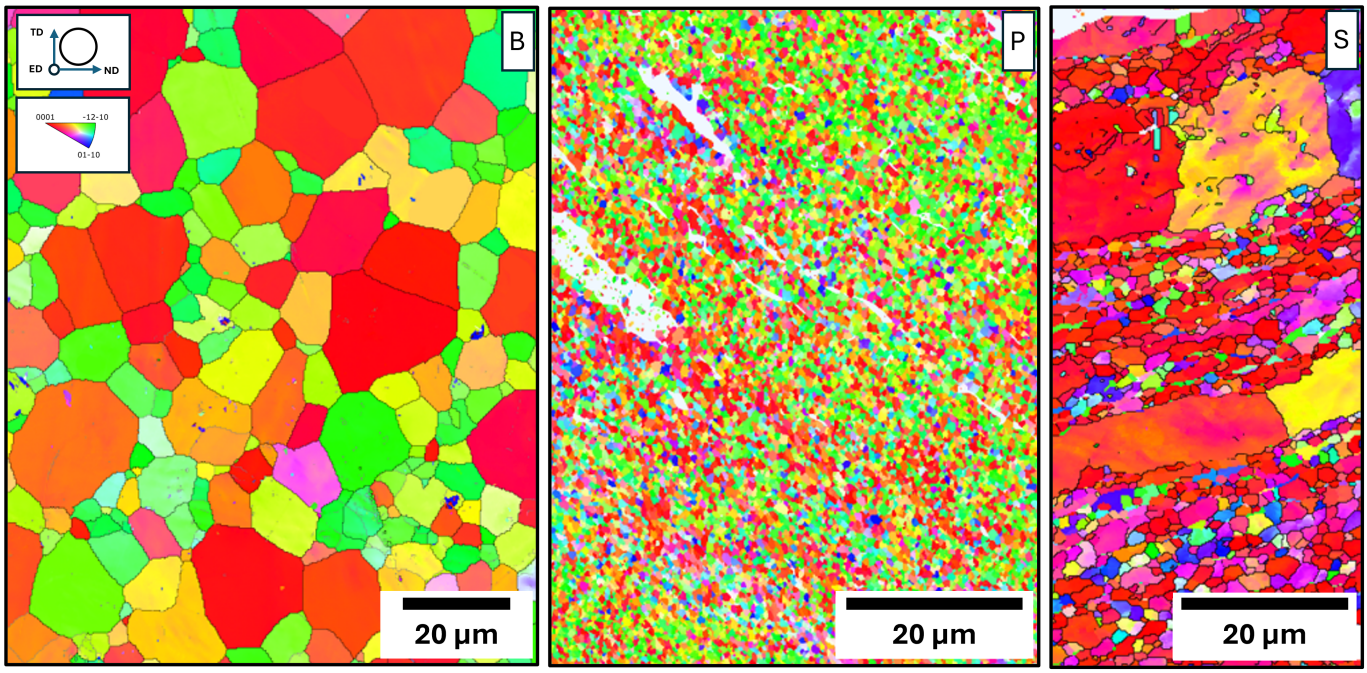
Table 1. Results of the chemical analysis testing showing the oxygen, carbon and nitrogen content of the wire produced from the different sources.

Feedstock	Sample	Oxygen (wt.%)	Carbon (wt.%)	Nitrogen (wt.%)
Bar	1	0.17	0.016	0.012
	2	0.19	0.017	0.011
	3	0.16	0.018	0.010
Powder	1	0.42	0.056	0.052
	2	0.43	0.068	0.057
	3	0.39	0.062	0.034
Swarf	1	0.13	0.047	0.016
	2	0.098	0.024	0.012
	3	0.11	0.028	0.004

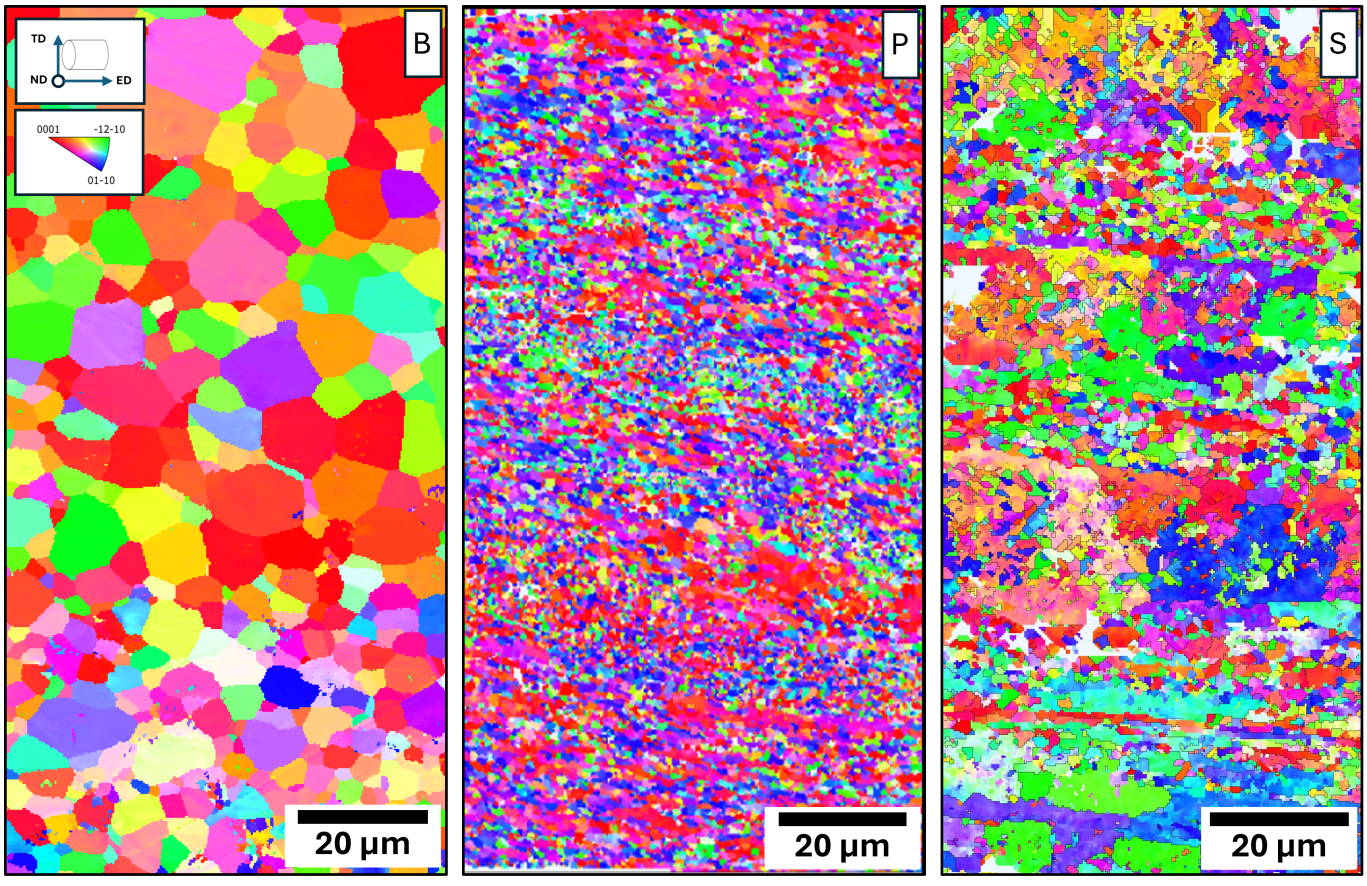


(**a**) (**b**)

Figure 11. (**a**) The 5 mm height EBSD of the wire. (**b**) The 5 mm height cross-polarized micrographs of the wire (B—bar, P—powder, and S—swarf).



(**a**)



(**b**)

Figure 12. EBSD IPF Z analysis of the three produced wire samples. (**a**) Analysis along the extrusion direction of the sample. (**b**) Analysis along the transverse direction of the sample (B—bar, P—powder, and S—swarf).

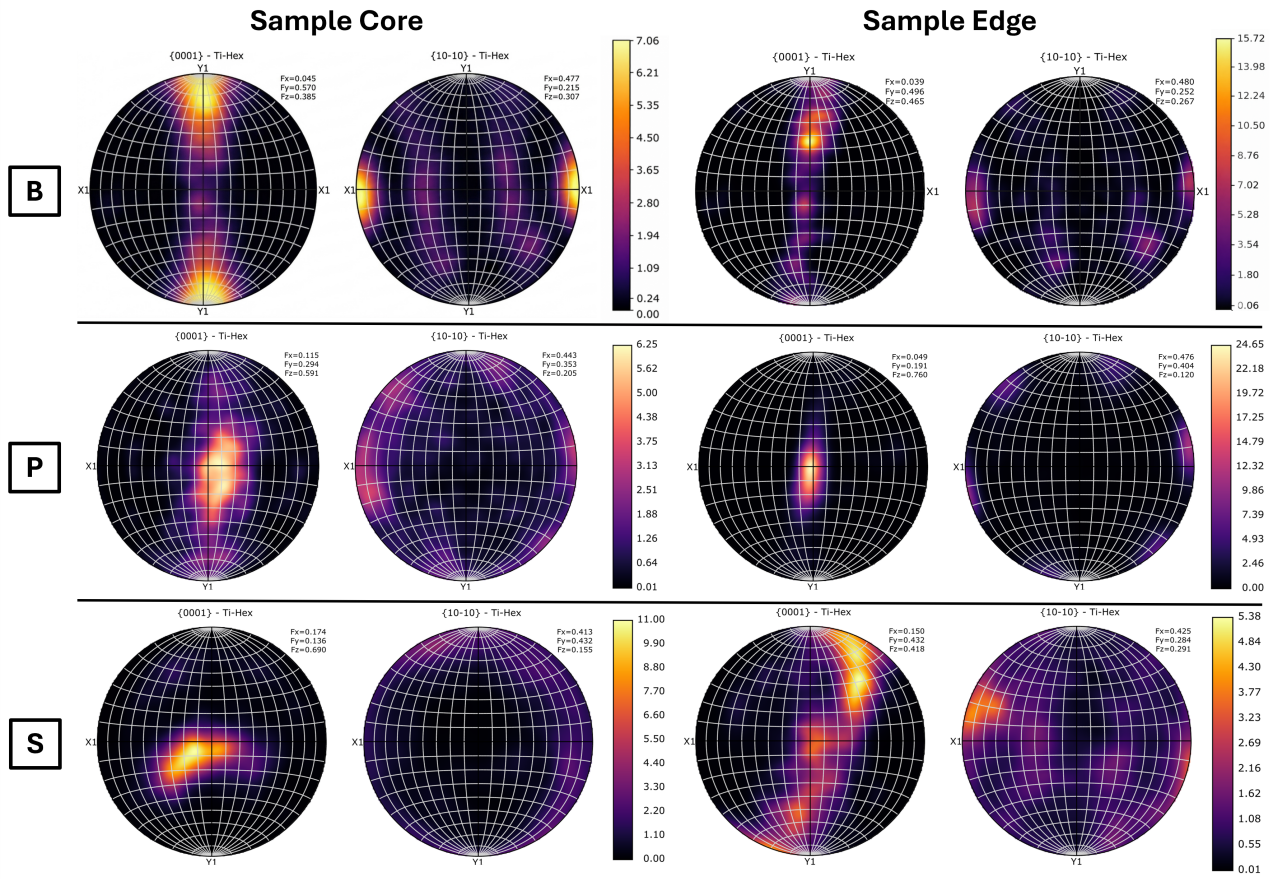


Figure 13. Pole figures of the sample cores and edges of all three produced wire sources (Y1 extrusion direction). B—bar, P—powder, and S—swarf.

3.4. Mechanical Performance of the Extruded Wire

3.4.1. Tensile Behavior

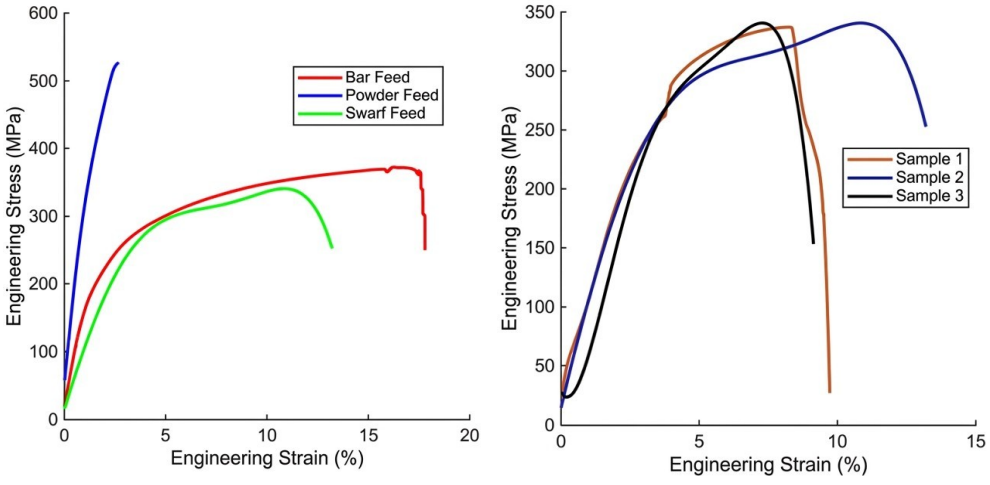
Tensile testing was performed on the samples in the as-produced condition before any heat treatments. From the tensile testing data in Table 2 it can be seen that, of the three feedstocks, the bar-derived wire had the best balance of tensile properties. This was the expected outcome as this is the optimized feedstock type for the CONFORM™ wheel and tooling geometry and set-up. The extruded wire deriving from powder has demonstrated an extremely high UTS with extremely low elongation. With an optimized post-extrusion heat treatment of the entire wire sample this could lead to a very good combination of properties that could rival that of the bar sample. The swarf samples show a very varied set of results, with a relatively consistent UTS for all the samples around 340 MPa. This is similar to that of the bar, which is very promising, but there are issues faced by the elongation of the wire samples. Overall the elongation of the swarf-derived wire is generally lower than that of the bar sample, with the worst being half that of one of the bar samples. However, there are promising results in samples 1 and 2. These wire samples show much higher elongation than the other swarf samples, with sample 2 almost maintaining the same elongation as the bar-derived samples. This variation within all the wire types is likely due to the microstructural variation seen within the analyzed samples. The wires with lower elongation are likely to have large areas of sub-micron grains, which are areas where some pieces of the swarf have not fully bonded to the bulk material. This would lead to high stress concentrations in these areas and likely limit deformation slip, which the material can undergo, causing premature failure.

Table 2. Mechanical property comparison between bar, powder, and swarf samples. Values are presented as mean ± standard deviation (SD). Powder samples fractured before yield stress could be measured.

Feedstock	Sample	UTS (MPa)	Elongation (%)	Yield Stress (MPa)
Bar	1	362	15.0	278
	2	373	16.0	294
	Mean ± SD	367.5 ± 7.8	15.5 ± 0.7	286.0 ± 11.3
Powder	1	502	0.0	NA
	2	546	1.0	NA
	Mean ± SD	524.0 ± 31.1	0.5 ± 0.7	NA
Swarf	1	337	9.5	215
	2	350	14.0	276
	3	346	8.0	249
	Mean ± SD	344.3 ± 6.7	10.5 ± 3.1	246.7 ± 30.6

An analysis of the stress–strain curves in Figure 14 highlights the high strength that the powder-derived wire can have. The lack of ductility in the as-extruded wire is likely due to the high wheel speed causing a large amount of strain to be imparted into the wire. With further optimization of the production process with a lower speed and higher temperature and an argon shroud, a larger grain size can be produced. Secondly the similarities between the curves of both the bar- and swarf-derived wire are very optimistic outcomes of these trials. The similarities in both the overall strain of the UTS and general shape from a completely unoptimized production show that there is a high likelihood that, with further development on both the tooling and production parameters, there will be very little difference between the overall performance of both samples.

Figure 14b highlights the main issue that is faced by further research into using swarf as a feedstock, which is variation between the samples. The curves show that the overall behavior of the samples follows a generally consistent pattern up to the UTS, but samples 1 and 3 follow a sharp decline once they reach their UTS. Sample 2, however, follows a more controlled ductile fracture towards failure. This is further evidence that the failure of these samples is more than likely due to the ultra-fine-grain regions causing sudden failure of the samples. If a more homogeneous microstructure can be produced, swarf samples could show similar properties to the bar feedstock.



(**a**) (**b**)

Figure 14. Stress–strain graphs for the 3 different feedstocks. (**a**) Comparison of the best-performing wire produced from each feedstock. (**b**) The three samples produced via swarf.

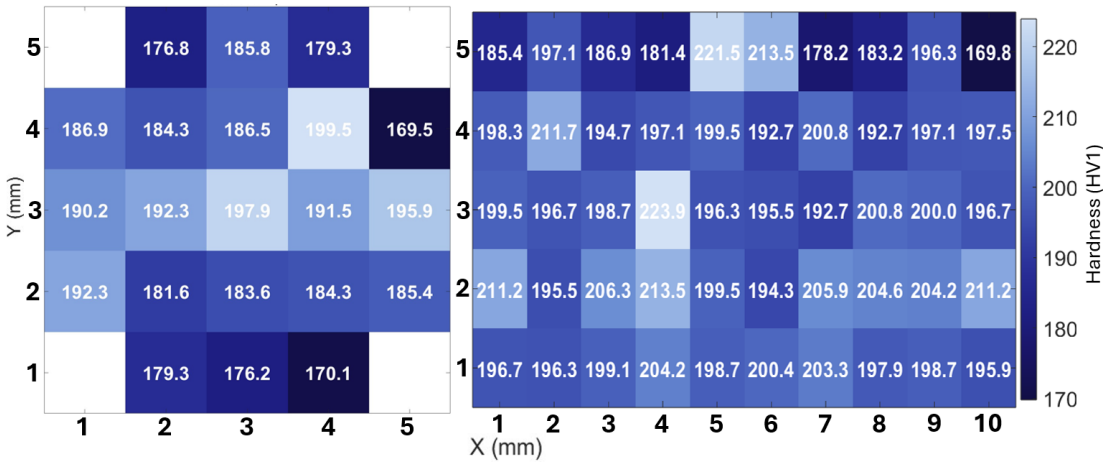
3.4.2. Hardness Testing

The hardness testing results are shown in Figure 15 for all three of the wire sample types. The hardness towards the edge of all three wire sample types is higher than that of the core of the samples. This is due to the increase in the strain that has been predicted from the modeling. This result is not completely consistent as there are some areas of the samples, especially within the bar and swarf, that demonstrate very low hardness. This is likely due to material being stagnated in the die chamber and exposed to higher temperatures. The bar samples show the most consistent hardness with a range of around 60 HV1 between the highest and lowest values. The powder-derived wire also shows a relatively consistent hardness over most of the sample. This sample also shows the highest surface hardening effect compared to the other wire samples. The swarf-derived wire sample has a very varied range of hardness values due to the micro-grains seen in the sample. Interestingly the hardness of these areas is noticeably higher than that of the powder sample, which demonstrates the effect these areas could have on the overall ductility of the samples. It also demonstrates how these areas are focused generally towards the edge of the sample and do not impinge on the core of the sample in the extrusion direction. In addition, in the transverse direction of the swarf sample, the high-hardness regions follow the flow lines in the micrographs observed in Figure 11b. Unlike the previous bar- and powder-derived wire, the transverse direction has much larger areas of higher hardness towards the core of the sample with very low hardness on the bottom edge. This may be due to the differing hardness of the initial swarf particles, but further work is required to confirm this.

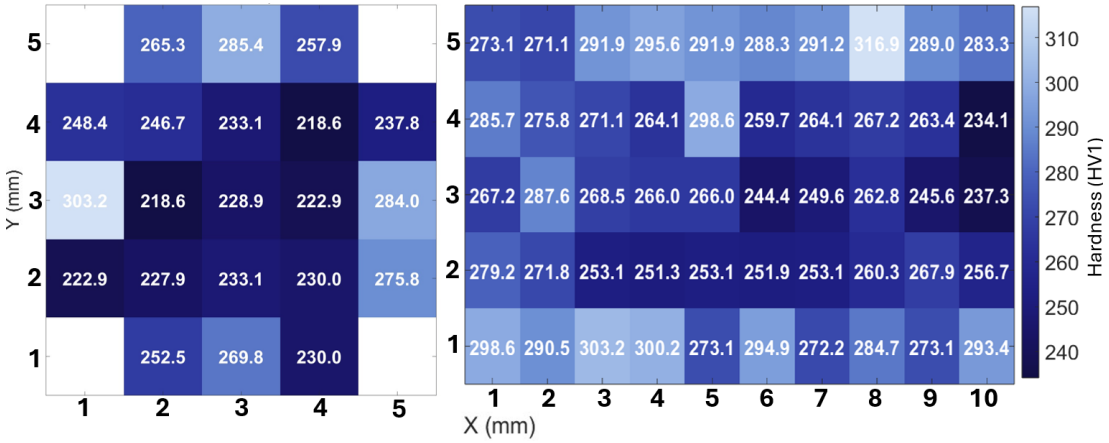
Overall the hardness of the swarf samples is generally lower than that of the bar- or powder-derived wire samples. With such a range in hardness it is challenging to determine whether the hardness evolution has occurred from processing or the initial hardness of the swarf particles is dominating. In these areas that have retained sub-micron grain sizes, it may be due to a poor bond with the material around it. If this is the case, then increases in processing temperature and wheel speed may reduce this issue. The authors determined that this is another area that will require further analysis to assess the effect of the process to guarantee wire quality. This will ensure consistency of production. Understanding the effects of the process on the hardness specifically of the swarf-derived wire will help if the material is to be used in its as-produced form or if further processing is needed following production.

3.5. Fractography

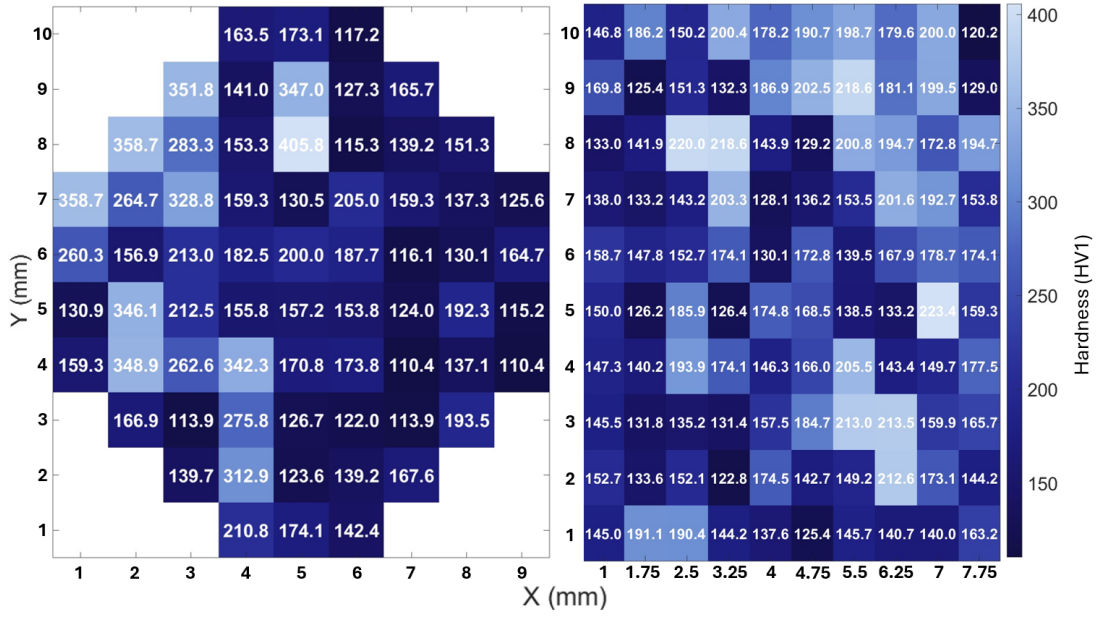
The fracture surfaces are shown in Figure 16 for all the wire types with some of the expected results from the tensile results of the samples. The samples that were used to analyze the fracture surfaces are the same samples that show the best set of mechanical properties from each produced wire type. The initial bar sample (Figure 16a) shows the necking, which can be seen from the side of the sample, with a very even fracture surface showing a clean ductile fracture and no areas displaying brittle behavior. The powder-derived wire sample shows the outer layer of the material detaching from the core of the material, with some areas ranging between 200 and 350 μm thick, as can be observed in Figure 16b.



(**a**)

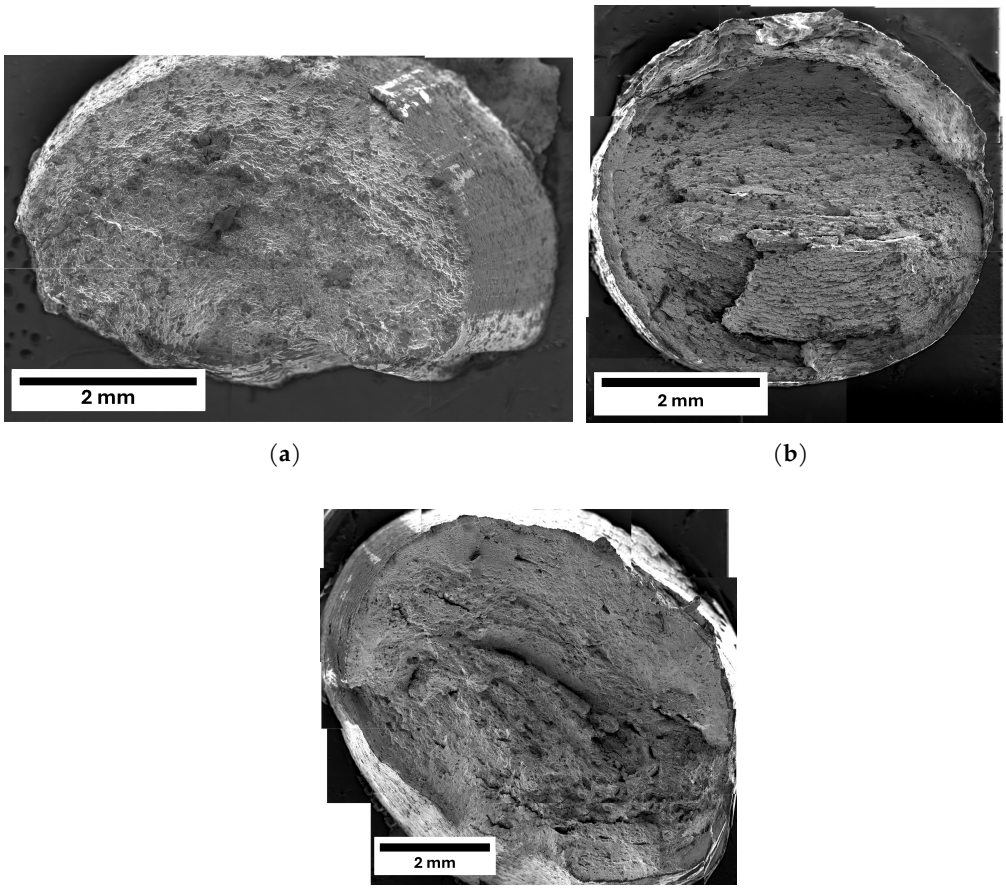


(**b**)



(**c**)

Figure 15. Hardness maps of the three produced wire samples. Extrusion direction and transverse direction: (**a**) 5 mm bar-derived wire, (**b**) 5 mm powder-derived wire, and (**c**) 10 mm swarf-derived wire.



(**a**) (**b**)

(**c**)

Figure 16. Secondary electron images of the fracture surfaces of the three samples shown in Figure 14b. (**a**) Bar-derived wire, (**b**) powder-derived wire, and (**c**) swarf-derived wire.

This is an issue that can be seen with CONFORM™ processing when the speed of the wheel and the tooling temperature are both too low. This leads to incomplete diffusion bonding of the powder at the edges of the die, which tends to spill out rather than completely consolidate, leading to this issue. The rest of the sample shows a very brittle fracture surface, as expected from the very low elongation and almost no evidence of necking. However, again, it seems that the major cause of the fracture was the edge surfaces. With an increased temperature of production it is likely that this would increase the elongation and ductility of the sample. As for the swarf-derived wire (Figure 16c) there is evidence of mixed-mode fracture from the surface, with a small region of brittle fracture upon the edge of the sample where the small-grain regions are usually seen in the swarf material. The variation observed on the surface coincides with the results of the hardness testing of the sample, where some regions show much higher hardness, thereby leading to lower levels of ductility in the wire. However, aside from this, the sample shows a good amount of necking and very little evidence of inclusions within the produced wire. This further highlights that fixing the inconsistency of producing the swarf wire through further research can lead to the production of high-quality wire stock.

4. Conclusions

One of the major outcomes of these trials is the demonstration of the closed-loop recycling process that can be performed with CONFORM™. Demonstrating the ability to produce CONFORM™ tooling from recycled nickel superalloy powder from the aerospace sector via the FAST process twinned with the use of machining swarf from aerospace waste

allows CONFORM™ to operate almost entirely from secondary sources of aerospace waste. The FAST process demonstrated an efficient method for the production of CONFORM™ abutment tooling, which could be exploited to reduce lead times and the reliance on external sources of conventional superalloy forgings.

A major aspect of this study is also the carbon footprint of this project, which is based entirely within the South Yorkshire region of the UK. This shows the ability to reduce the environmental impact and cost of titanium production and allows the use of materials that are processed within the UK from waste sources, which can include waste from additive manufacture or swarf from machining, which are much more economically viable than materials from primary production sources. It also massively reduces the supply chain that the material has to go through before processing, simply requiring washing and sorting, enabling subsequent use directly within CONFORM™ to produce high-quality low-cost wire.

The success of the CONFORM™-manufactured wire from this material demonstrates the full consolidation and robust nature of the tooling produced via the FAST process and that these materials can aid the development of the process. The use of recycled materials for tooling purposes makes the process much more economically safe as it reduces user reliance on primary sources of material extraction, allowing much more independence from primary sources, which can be heavily affected by world politics and events. This is especially true for countries like the UK, which have limited sources of primary titanium and rely on imports but have very large sources of secondary material. Due to a large aerospace manufacturing base, around 90% of the titanium is machined away from forgings, leading to an abundance of sustainable feed material and allowing the production of wire with little to no previous material processing [5].

Future trials on the CONFORM™ process will focus on the development of the wire from both powder and swarf sources, specifically focusing on optimization through ideas gained from these trials. This will include reducing the swarf particle size distribution that is used within the process to reduce the blockages in the feed system when producing wire from swarf. It is also hoped that this particle size reduction will have an effect on the larger prior swarf particles that remain distinct in the bulk material by allowing improved consolidation and breaking the surface oxides of the material. The temperature will be increased during the production of both the wheel and die to reduce the flow stress of the material and then examine the effects of the increase in the oxygen content of the produced wire. It is hoped that these changes will produce a more consistent internal microstructure, surface finish and mechanical properties to make the produced wire more industrially viable and allow future research into the possible production of a relationship between the wheel speed, tooling temperature and produced grain size of the wire.

Author Contributions: Conceptualization, M.J.; methodology, L.C. and M.J.; software, L.C.; validation, L.C.; formal analysis, L.C.; investigation, L.C., S.L., W.P. and E.G.; resources, M.J., W.P. and E.G.; data curation, L.C.; writing—original draft preparation, L.C. and S.L.; writing—review and editing, L.C., M.J. and S.L.; visualization, L.C.; supervision, M.J.; project administration, M.J.; funding acquisition, M.J. All authors have read and agreed to the published version of the manuscript.

Funding: This research was funded by the Engineering Physical Sciences Research Council's Advance Metallic Systems Centre for Doctoral Training and by the Defence Science and Technology Laboratory (Dstl), UK. Funding was also provided by Science Foundation Ireland (18/EPSRC-CDT/3584) and the Engineering and Physical Sciences Research Council UK (EP/S022635/1) through the Advanced Metallic Systems Centre for Doctoral Training (EP/R00661X/1, EP/P02470X/1, EP/S019367/1 & EP/X52850X/1).

Data Availability Statement: The datasets presented in this article are not readily available because the data is part of an ongoing research project.

Acknowledgments: The authors would like to thank Nigel Adams and Jorge Elkin for technical support and discussions with the FAST and CONFORM™ processes. We also acknowledge Luke Rumsey and Matthew Lunt from DSTL for participating in technical discussions and helping to promote the recycling industry.

Conflicts of Interest: The authors declare no conflicts of interest. The funders had no role in the design of the study; in the collection, analyses, or interpretation of data; in the writing of the manuscript; or in the decision to publish the results.

Abbreviations

The following abbreviations are used in this manuscript:

FAST	Field-Assisted Sintering Technology
SPD	Severe Plastic Deformation
CP-Ti	Commercially Pure Titanium
AM	Additive Manufacturing
ECAP	Equal Channel Angular Processing
WAAM	Wire Arc Additive Manufacture
AFSD	Additive Friction Stir Deposition

References

1. Hurless, B.E.; Froes, F. Lowering the Cost of Titanium. *AMPTIAC Q*. **2002**, *6*, 3–8.
2. Gerdemann, S. Titanium Process Technologies. *Adv. Mater. Processes* **2001**, *159*, 41.
3. Kraft, H.E. *Summary of Emerging Low Cost Titanium Technologies EHKTechnologies*; Technical Report; Oakridge National Laboratory: Vancouver, BC, Canada, 2004.
4. Feng, E.; Gao, D.; Wang, Y.; Yu, F.; Wang, C.; Wen, J.; Gao, Y.; Huang, G.; Xu, S. Sustainable recovery of titanium from secondary resources: A review. *J. Environ. Manag.* **2023**, *339*, 117818. [CrossRef] [PubMed]
5. Klocke, F.; Arntz, K.; Klingbeil, N.; Schulz, M. Wire-based laser metal deposition for additive manufacturing of TiAl6V4: Basic investigations of microstructure and mechanical properties from build up parts. In *Laser 3d Manufacturing*, 4th ed.; Gu, B., Helvajjan, H., Piqué, A., Dunsky, C.M., Liu, J., Eds.; SPIE: Bellingham, WA, USA, 2017; Volume 10095, p. 100950U. [CrossRef]
6. Shial, S.R.; Masanta, M.; Chaira, D. Recycling of waste Ti machining chips by planetary milling: Generation of Ti powder and development of in situ TiC reinforced Ti-TiC composite powder mixture. *Powder Technol.* **2018**, *329*, 232–240. [CrossRef]
7. Weston, N.S.; Jackson, M. FAST-Forge: A new cost-effective hybrid processing route for consolidating titanium powder into near net shape forged components. *J. Mater. Process. Technol.* **2017**, *243*, 335–346. [CrossRef]
8. Li, Y.; Su, C.; Zhu, J. Comprehensive review of wire arc additive manufacturing: Hardware system, physical process, monitoring, property characterization, application and future prospects. *Results Eng.* **2022**, *13*, 100330. [CrossRef]
9. Rodrigues, T.A.; Duarte, V.; Miranda, R.M.; Santos, T.G.; Oliveira, J.P. Current status and perspectives on wire and arc additive manufacturing (WAAM). *Materials* **2019**, *12*, 1121. [CrossRef] [PubMed]
10. Estrin, Y.; Vinogradov, A. Extreme grain refinement by severe plastic deformation: A wealth of challenging science. *Acta Mater.* **2013**, *61*, 782–817. [CrossRef]
11. Segal, V.M. Severe plastic deformation: Simple shear versus pure shear. *Mater. Sci. Eng.* **2001**, *338*, 331–344. [CrossRef]
12. Faraji, G.; Seop Kim, H.; Kashi Torabzadeh, H. *Severe Plastic Deformation*, 1st ed.; Elsevier Science: Tehran, Iran, 2018; Volume 1, pp. 19–97.
13. Azushima, A.; Kopp, R.; Korhonen, A.; Yang, D.Y.; Micari, F.; Lahoti, G.D.; Groche, P.; Yanagimoto, J.; Tsuji, N.; Rosochowski, A.; et al. Severe plastic deformation (SPD) processes for metals. *CIRP Ann.-Manuf. Technol.* **2008**, *57*, 716–735. [CrossRef]
14. Chouhan, D.K.; Komarasamy, M.; Taysom, S.B.; Overman, N.R.; Canfield, N.L.; Roosendaal, T.J.; Reynolds, A.P.; Whalen, S.A. Friction-based recycling: An evaluation of friction extrusion for fabricating Ti-6Al-4 V wire fabricated from machining chip feedstock. *Int. J. Adv. Manuf. Technol.* **2025**, *137*, 2519–2528. [CrossRef]
15. Valiev, R.Z.; Langdon, T.G. Principles of equal-channel angular pressing as a processing tool for grain refinement. *Prog. Mater. Sci.* **2006**, *51*, 881–981. [CrossRef]
16. Qi, Y.; Timokhina, I.B.; Shekhter, A.; Sharp, K.; Lapovok, R. Optimization of upcycling of Ti-6Al-4V swarf. *J. Mater. Process. Technol.* **2018**, *255*, 853–864. [CrossRef]
17. Zhu, Y.T.; Lowe, T.C. Observations and issues on mechanisms of grain refinement during ECAP process. *Mater. Sci. Eng.* **2000**, *291*, 46–53. [CrossRef]
18. Xu, C.; Furukawa, M.; Horita, Z.; Langdon, T.G. The evolution of homogeneity and grain refinement during equal-channel angular pressing: A model for grain refinement in ECAP. *Mater. Sci. Eng. A* **2005**, *398*, 66–76. [CrossRef]

19. Green, D. Improvements in or relating to extrusion. UK Patent 1370894,US3765216A, Granted 16 October 1973.
20. Etherington, C. *Conform and The Recycling of Non-Ferrous Scrap Metals**; Technical Report; Springfields Nuclear Power Development Laboratories: Lancashire, UK, 1978.
21. Childerhouse, T.; Jackson, M. Near net shape manufacture of titanium alloy components from powder and wire: A review of state-of-the-art process routes. *Metals* **2019**, *9*, 689. [CrossRef]
22. Henly, A. Conform-Continuous Extrusion of Powder Products. *Met. Powder Rep.* **1991**, *46*, 44–47. [CrossRef]
23. Thomas, B.M.; Derguti, F.; Jackson, M. Continuous extrusion of a commercially pure titanium powder via the Conform process. *Mater. Sci. Technol.* **2017**, *33*, 899–903. [CrossRef]
24. Pardoe, J.A. Conform continuous extrusion of metal powders into products for electrical industry: Development experience. *Powder Metall.* **1979**, *22*, 22–28. [CrossRef]
25. Kim, Y.H.; Cho, J.R.; Jeong, H.S.; Kim, K.S.; Yoon, S.S. A study on optimal design for CONFORM process. *J. Mater. Process. Technol.* **1998**, *80–81*, 671–675. [CrossRef]
26. Thomas, P.; Scott, K. From particles to solids: "Conform" for recycling and special alloys. *Alum. Int. Today* **2003**, *15*, 36–38.
27. Smythe, S.A.; Thomas, B.M.; Jackson, M. Recycling of titanium alloy powders and swarf through continuous extrusion (Conform™) into affordable wire for additive manufacturing. *Metals* **2020**, *10*, 843. [CrossRef]
28. Weston, N.S.; Jackson, M. FAST-Forge of titanium alloy swarf: A solid-state closed-loop recycling approach for aerospace machining waste. *Metals* **2020**, *10*, 296. [CrossRef]
29. Lin, Z.; Song, K.; Yu, X. A review on wire and arc additive manufacturing of titanium alloy. *J. Manuf. Processes* **2021**, *70*, 24–45. [CrossRef]
30. Lebot, R.; Saly, E.; Mellier, D.; Sallot, P.; huser, G.; Villechaise, P.; Cormier, J. Ductility Dependence of a Ni-Based Superalloy Made by Spark Plasma Sintering on Prior Particle Boundaries and Grain Size. *Metall. Mater. Trans. A Phys. Metall. Mater. Sci.* **2026**, *57*, 1975–1989. [CrossRef]
31. Lin, C.I.; Yamamoto, N.; King, D.S.; Singh, J. Solid-State Joining of Dissimilar Ni-Based Superalloys via Field-Assisted Sintering Technology for Turbine Applications. *Metall. Mater. Trans. A Phys. Metall. Mater. Sci.* **2021**, *52*, 2149–2154. [CrossRef]
32. Lister, S.; Blanch, O.L.; Fernandez, D.S.; Pope, J.; Baxter, G.J.; Bray, S.; Jackson, M. A Machinability Assessment of the Novel Application of Field-Assisted Sintering Technology to Diffusion Bond (FAST-DB) and Functionally Grade Dissimilar Nickel-Based Superalloys. *Metall. Mater. Trans. A Phys. Metall. Mater. Sci.* **2023**, *54*, 4396–4408. [CrossRef]
33. Marshall, K.; Schillinger, P.; Weston, N.S.; Epler, M.; Jackson, M. A parametric study of the microstructural evolution of an advanced Ni-based superalloy powder when consolidated using Field Assisted Sintering Technology, compared to a hot isostatic pressing benchmark. *Adv. Ind. Manuf. Eng.* **2022**, *5*, 100103. [CrossRef]
34. Krohn, J.; Pepper, J.; Jackson, M. The Influence of Field-Assisted Sintering Technology (FAST) Temperature and Cooling Rate on the Microstructural Evolution in Gamma-Titanium Aluminide Alloy GE4822. *Adv. Eng. Mater.* **2026**, *28*, e71126. [CrossRef]
35. *BS EN 2002-1:2005*; Aerospace Series. Metallic Materials. Test Methods. Tensile Testing at Ambient Temperature. British Standards Institutions (BSI): London, UK, 2006.
36. Yang, Z.; Tang, J.; Mo, X.; Chen, W.; Fu, D.; Zhang, H.; Teng, J.; Jiang, F. Microstructure, mechanical properties, and strengthening mechanisms of ultra-high strength Al-Zn-Mg-Cu alloy prepared by continuous extrusion forming process. *Mater. Des.* **2024**, *242*, 112985. [CrossRef]

Disclaimer/Publisher's Note: The statements, opinions and data contained in all publications are solely those of the individual author(s) and contributor(s) and not of MDPI and/or the editor(s). MDPI and/or the editor(s) disclaim responsibility for any injury to people or property resulting from any ideas, methods, instructions or products referred to in the content.